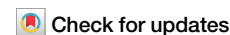


<https://doi.org/10.1038/s41746-025-01891-w>

# Preserving the first ray or first two rays in forefoot amputation for diabetic foot ulcers



Wei Mao<sup>1,2,3,4,6</sup>✉, Da-Jun Jiang<sup>1,6</sup>, Ying-Qi Zhang<sup>4,5,6</sup>, Khin Yee Sammy Loh<sup>2,3</sup>, Yi-Ming Qi<sup>4</sup>, Shi-Min Chang<sup>4</sup>, Wei-Tao Jia<sup>1</sup>✉ & Choon Chiet Hong<sup>2,3</sup>✉

Approximately 20% of diabetic foot ulcers (DFUs) patients require lower extremity amputation, and postoperative reulceration and reamputation remains common. To clarify the biomechanical consequences and reulceration risk of different ray amputations (RAs), we built finite-element models and simulated various RAs. During the simulated gait cycle, amputation of the first ray or first two rays (1 RA and 1-2 RA) exhibited higher von Mises stress and strain values. These two RAs also generated larger plantar “danger areas” for reulceration, suggesting that 1 RA and 1-2 RA may substantially increase reulceration risk. Conversely, preserving the first ray or first two rays mitigates reulceration risk. Two clinical case examples aligned with the modelling results. This study concludes that, when feasible, preserving the first ray or first two rays helps maintain foot biomechanics and reduces reulceration risk; if 1 RA or 1-2 RA is unavoidable, transmetatarsal amputation might be more suitable.

Diabetic foot ulcers (DFUs), a common complication of diabetes mellitus, represent a global clinical challenge that is comparable to cancer in terms of chronicity, recidivism, cost, and burden<sup>1–4</sup>. In 2020, the International Diabetes Federation estimated that between 40 to 60 million patients worldwide suffer from DFUs, marking a surge from the 9 to 26 million estimated in 2015<sup>5</sup>.

Roughly 20% DFU patients will require some level of lower extremity amputation<sup>1</sup>. Among those who have undergone DFU amputation, approximately 40% experience ulcer recurrence within 1 year after ulcer healing, almost 60% within 3 years, and 65% within 5 years<sup>6</sup>. Therefore, when determining the level of foot amputation, the challenge lies in striking a balance between minimizing the risk of reulceration, and preserving as much of the foot’s load-bearing capacity as well as ensuring better functional ambulation<sup>6,7</sup>. In the treatment of severe forefoot DFUs, transmetatarsal amputation (TMA) is a well-recognized surgical procedure, involving extensive removal of the forefoot at the level of metatarsal shafts<sup>8</sup>. TMA effectively prevents the forefoot infection and necrosis from spreading to the other parts of the limb, thereby contributing to long-term limb preservation<sup>8,9</sup>. On the other hand, some prefer a more minor surgery such as the ray amputation (RA)—the resection of the toe and the metatarsal head—removing inviable rays and trying to preserve viable rays, retaining more functionality for patients’ ambulation and balance<sup>10</sup>. Although RA is a commonly performed procedure on affected rays, it has been questioned for

potentially increasing the risks of reulceration and reamputation in the residual forefoot stump<sup>11–13</sup>. In a meta-analysis of 21 studies with 483 patients, Sanz et al.<sup>14</sup> found a significant correlation between RA treatment for DFUs and increased reulceration rates. Consequently, a long-asked question persists in the management of severe forefoot DFUs: Which types of RA have a lower risk of reulceration and thereby offering greater durability?

Previous clinical reports are mainly single-center studies with small sample sizes, and the conclusions from different studies are conflicting, thus providing limited evidence for clinical intervention<sup>15–19</sup>. McGuire et al.<sup>15</sup> concluded that the first ray amputation (1 RA) or the fifth ray amputation (5 RA) typically resulted in better outcomes, whereas resection of central rays (2 or 3 or 4 RA) was significantly associated with reulceration. Conversely, in a prospective analysis of 119 patients with DFUs, Molines et al.<sup>16</sup> observed that the 1 RA group had highest risk of reulceration and the 5 RA group had the lowest risk. Moreover, in a prospective analysis of 65 patients, García et al.<sup>17</sup> reported that in cases of first and second rays amputation (1-2 RA), increase of plantar pressure was a predictor of reulceration.

Recent advances in computational simulation have emerged as a powerful tool to analyze biomechanical behavior of feet<sup>20,21</sup>. For instance, Shaulian et al.<sup>22</sup> utilized finite element (FE) analysis to optimize the design of offloading footwear insoles, enhancing their effectiveness in preventing and

<sup>1</sup>Department of Orthopaedics, Shanghai Sixth People’s Hospital Affiliated to Shanghai Jiao Tong University School of Medicine, Shanghai, China. <sup>2</sup>Department of Orthopaedic Surgery, National University Hospital, National University Health System, Singapore, Singapore. <sup>3</sup>Department of Orthopaedic Surgery, Yong Loo Lin School of Medicine, National University of Singapore, Singapore, Singapore. <sup>4</sup>Department of Orthopaedic Surgery, Yangpu Hospital, School of Medicine, Tongji University, Shanghai, China. <sup>5</sup>Department of Orthopaedics, Tongji Hospital, School of Medicine, Tongji University, Shanghai, China. <sup>6</sup>These authors contributed equally: Wei Mao, Da-Jun Jiang, Ying-Qi Zhang. ✉ e-mail: [dr.mao.wei@gmail.com](mailto:dr.mao.wei@gmail.com); [jiaweitao@shsmu.edu.cn](mailto:jiaweitao@shsmu.edu.cn); [choonchiet@gmail.com](mailto:choonchiet@gmail.com)

treating DFUs. Moreover, Jannel et al.<sup>23</sup> applied FE analysis to explore challenging biomechanical scenarios about the foot structure of sauropod dinosaurs, focusing on how their feet supported the gigantic body. Similarly, given that DFUs usually result from repetitive stress over an area that is subject to high stress in patients with peripheral neuropathy<sup>6</sup>, computational simulation can also be employed to investigate the risk of reulceration after RA procedure. Nevertheless, to the best of our knowledge, there was no FE analysis study on the foot biomechanics of different types of RA.

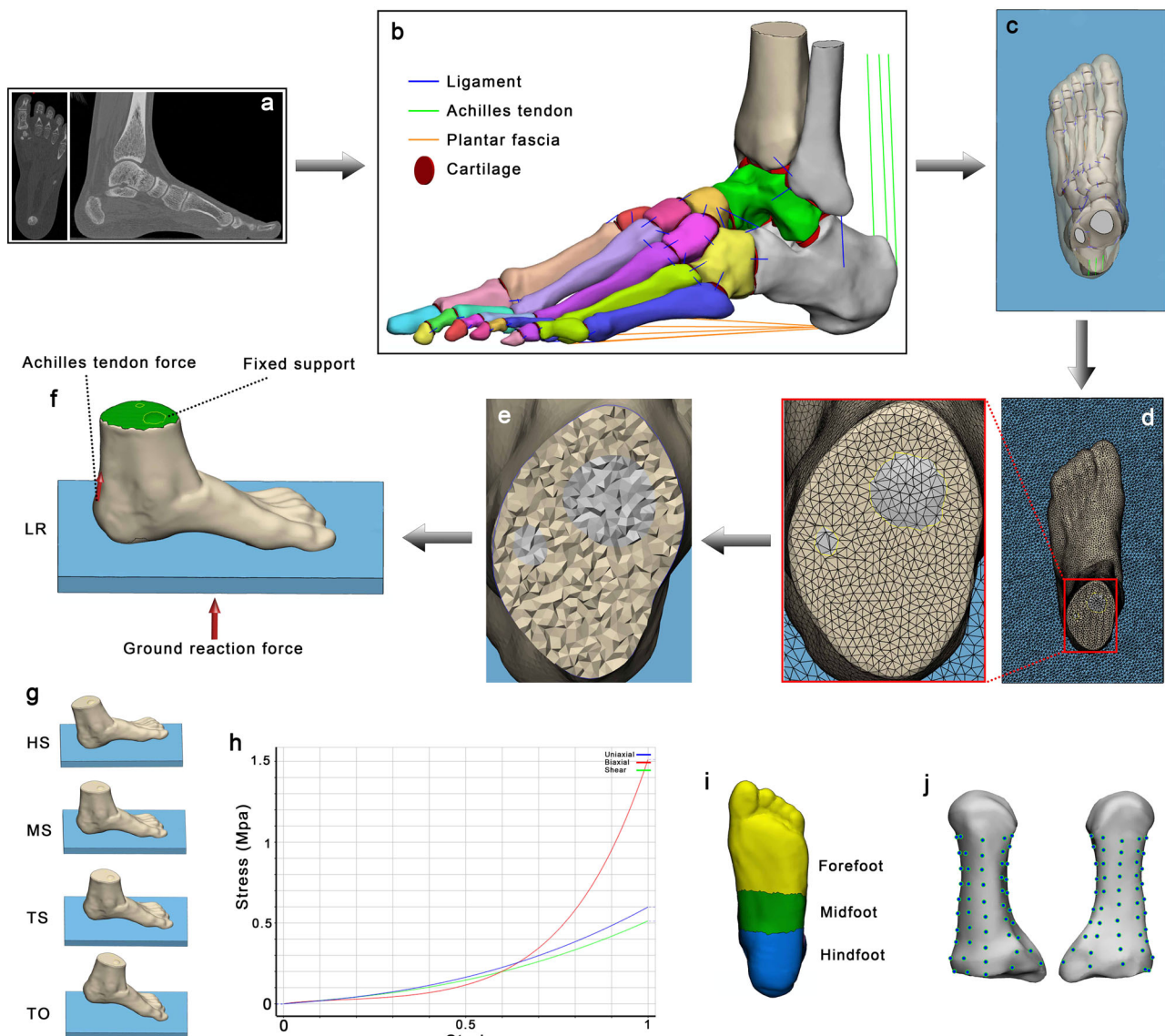
This study harnessed the precision of computational models to evaluate how various RA types affect foot biomechanics. By constructing a suite of FE diabetic foot models (Fig. 1), we were able to analyze the distribution and magnitude of stress and strain across different foot segments, thereby shedding light on the advantages and disadvantages of different RA types in terms of reulceration risk. Additionally, corresponding clinical case examples of RA procedures were used to corroborate the FE models, highlighting the study's clinical relevance. Ultimately, this study aims to contribute to a

more nuanced and biomechanically informed forefoot amputation decision-making framework, thus optimizing outcomes for DFU patients.

## Results

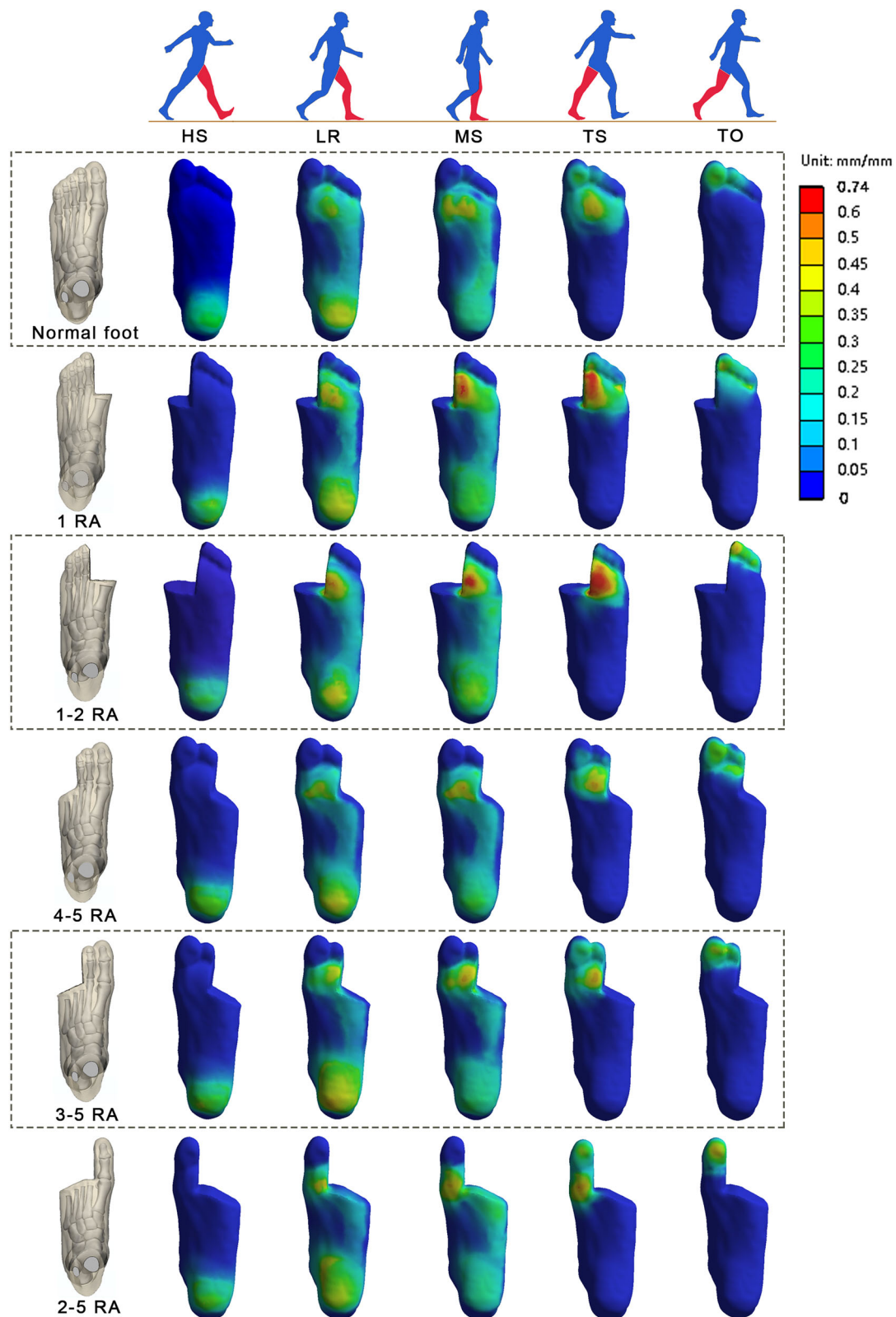
### The von Mises strain of the plantar foot

Figure 2 illustrated the distribution of von Mises strain across the plantar foot during a gait cycle. Regarding the regions of strain concentration, all six models displayed similar trends. In the first phase (heel strike, HS), the heel first contacted the ground, leading to a concentration of strain in the hindfoot. During the second phase (loading response, LR), this strain concentration spread across the entire foot. The third phase (middle stance, MS) marked the transition of strain concentration from the hindfoot to the forefoot. By the fourth phase (terminal stance, TS), the strain concentration had fully shifted to the forefoot, with each FE model reaching its maximal strain value in this phase. In the final phase (toe off, TO), the strain concentration was localized to the toes.



**Fig. 1 | Schematic diagram of finite element (FE) analysis.** **a** CT images of DICOM format were processed in Mimics software. **b** Models of bones were built based on CT data. Models of ligaments, Achilles tendon, plantar fascia, and cartilage were built based on anatomical landmarks. **c** Models of encapsulated soft tissue were built based on CT data. Ground plate models were created in 3-Matic software. **d** Surface face remeshing, wrapping and smoothing. **e** Constructing volume mesh. **f** After assigning

material property, loads and boundary constraints were set. The phase depicted here was the loading response (LR). **g** Models of other phases: heel strike (HS); middle stance (MS); terminal stance (TS); toe off (TO). **h** The strain-stress curve of the Mooney-Rivlin hyperelastic materials of the encapsulated soft tissue. **i** The plantar foot was partitioned into forefoot, midfoot, and hindfoot segments. **j** 80 nodes were marked on each metatarsal for von Mises stress measurement.



**Fig. 2 | The von Mises strain distribution across the plantar foot.** In five phases: heel strike (HS), loading response (LR), middle stance (MS), terminal stance (TS), toe off (TO), the overall strain levels in the 1 ray amputation (RA) and 1-2 RA groups were notably higher than those in other groups.

As depicted in Fig. 3a-c, danger values (mean von Mises strain  $>0.5$ ) for reulceration were only exhibited by the plantar forefoot. In contrast, both the midfoot and hindfoot displayed no indication of danger values. Within the forefoot, the Normal (control), 3-5 RA, and 4-5 RA groups showed no danger values, and the 1-2 RA, 1 RA, and 2-5 RA groups showed danger

values for reulceration. Table 1 indicated that the 1-2 RA group had three phases with danger values, and the highest danger values were all detected in the 1-2 RA group (LR:  $0.544 \pm 0.035$ , MS:  $0.639 \pm 0.037$ , TS:  $0.732 \pm 0.041$ ). In the 1 RA group, two phases (MS, TS) registered the danger values, while the maximal strain value of the LR phase ( $0.491 \pm 0.031$ ) was close to the



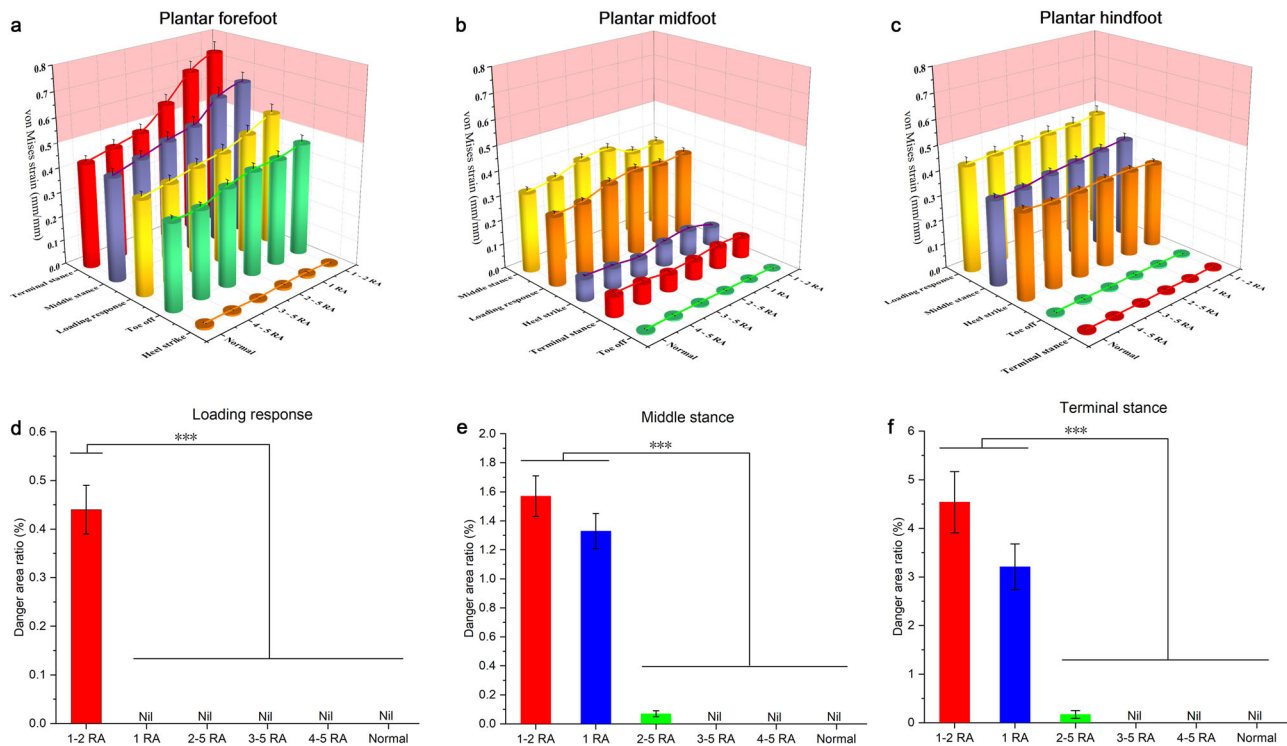


**Fig. 3 | Comparisons of von Mises strain values among six groups, comprising five ray amputation (RA) groups and one normal foot group. a** In the plantar forefoot, the 1-2 RA, 1 RA, and 2-5 RA groups showed danger values (mean von Mises strain > 0.5). Red backgrounds denote the danger threshold of 0.5, representing the safety margin of soft tissue. **b, c** The plantar midfoot and hindfoot

displayed no danger values. **d** In the phase of loading response, the 1-2 RA group was the sole group with danger area ratio. **e, f** In the phases of middle stance and terminal stance, the danger area ratios for the 1-2 RA and 1 RA groups were significantly higher than other groups ( $p < 0.001$ ). Data were presented as means  $\pm$  standard deviation.

**Table 1 | Groups and phases exhibiting danger values (mean von Mises strain > 0.5)**

Phase	1 RA	1-2 RA	2-5 RA
LR	/	0.544 $\pm$ 0.035	/
MS	0.605 $\pm$ 0.036	0.639 $\pm$ 0.037	0.516 $\pm$ 0.034
TS	0.678 $\pm$ 0.038	0.732 $\pm$ 0.041	0.571 $\pm$ 0.036

Danger values were not observed in the Normal (control), 3-5 RA, and 4-5 RA groups. The data were presented as mean  $\pm$  standard deviation.

RA, ray(s) amputation; LR, loading response; MS, middle stance; TS, terminal stance.

danger value threshold. The 2-5 RA group also had danger values in two phases (MS, TS), but they were significantly lower than those in the 1-2 RA ( $p < 0.001$ ) and 1 RA ( $p < 0.001$ ) groups.

Figure 3d–f displayed the danger area ratio (DAR, representing the percentage of the danger area of the total plantar foot area) of each group. During the LR phase, only the 1-2 RA group exhibited danger values, hence it was the only group with DAR. In the MS and TS phases, the DARs for the 1-2 RA and 1 RA groups were significantly higher than those of the 2-5 RA group ( $p < 0.001$ ). Besides, the Normal (control), 3-5 RA, and 4-5 RA groups showed no DARs.

### The von Mises stress of metatarsals

Figure 4 illustrated the von Mises stress distribution across the five metatarsals during the LR, MS, and TS phases. The stress conditions of the metatarsals indirectly indicated the stress conditions of the plantar soft tissues surrounding each metatarsal. Figure 5 and Table 2 display the von Mises stress on the marked nodes (Fig. 1j) of each metatarsal during the TS phase, allowing for a comparison of the stress levels between different metatarsals.

In the normal foot group, the 2nd metatarsal displayed the region of highest stress (Fig. 5a). The median value of von Mises stress was 20.03 MPa, with an interquartile range (IQR) of 11.12–28.06 MPa. The 3rd metatarsal exhibited the second highest stress level (median: 16.96 MPa, IQR: 7.73–26.54 MPa). Despite bearing much load, the 1st metatarsal showed low stress levels (median: 2.69 MPa, IQR: 1.16–4.69 MPa) (primarily because 1st metatarsal is thicker and shorter<sup>24</sup>).

In the 1 RA group, the stress level of the 1st metatarsal decreased (median: 2.18 MPa, IQR: 0.82–3.59 MPa). Due to the amputation of the 1st metatarsal and the subsequent load transfer laterally, stress levels of the 2nd (median: 25.79 MPa, IQR: 13.45–34.63 MPa), 3rd (median: 21.56 MPa, IQR: 12.88–30.86 MPa), 4th (median: 20.47 MPa, IQR: 11.63–30.49 MPa), and 5th (median: 20.47 MPa, IQR: 11.63–30.49 MPa) metatarsals markedly rose (Fig. 5b).

In the 1-2 RA group, compared to the normal foot group, stress levels of 1st metatarsals (median: 1.50 MPa, IQR: 0.64–2.81 MPa) and 2nd metatarsals (median: 2.50 MPa, IQR: 0.87–5.30 MPa) markedly dropped. Conversely, because of load transfer laterally, the 3rd (median: 29.30 MPa, IQR: 18.31–36.91 MPa), 4th (median: 26.46 MPa, IQR: 16.68–35.26 MPa), and 5th (median: 20.77 MPa, IQR: 11.08–30.56 MPa) metatarsals showed a pronounced increase in stress levels (Fig. 5c).

In the 4-5 RA group, the stress level of the 4th metatarsal markedly decreased (median: 2.98 MPa, IQR: 1.21–5.10 MPa). Due to load transfer medially, the stress level of the 3rd metatarsal increased (median: 20.87 MPa, IQR: 12.54–30.23 MPa). Meanwhile, the stress levels of the 1st (median: 3.28 MPa, IQR: 1.32–7.06 MPa) and 2nd (median: 20.18 MPa, IQR: 11.83–28.09 MPa) metatarsals remained relatively similar to those in the normal foot group (Fig. 5d).

In the 3-5 RA group, compared to the normal foot group, the stress levels of the 3rd (median: 2.08 MPa, IQR: 0.83–3.73 MPa) and 4th (median: 1.53 MPa, IQR: 0.55–2.80 MPa) metatarsals exhibited a significant decrease. There was a slight increase in the stress levels of the 1st (median: 5.07 MPa,

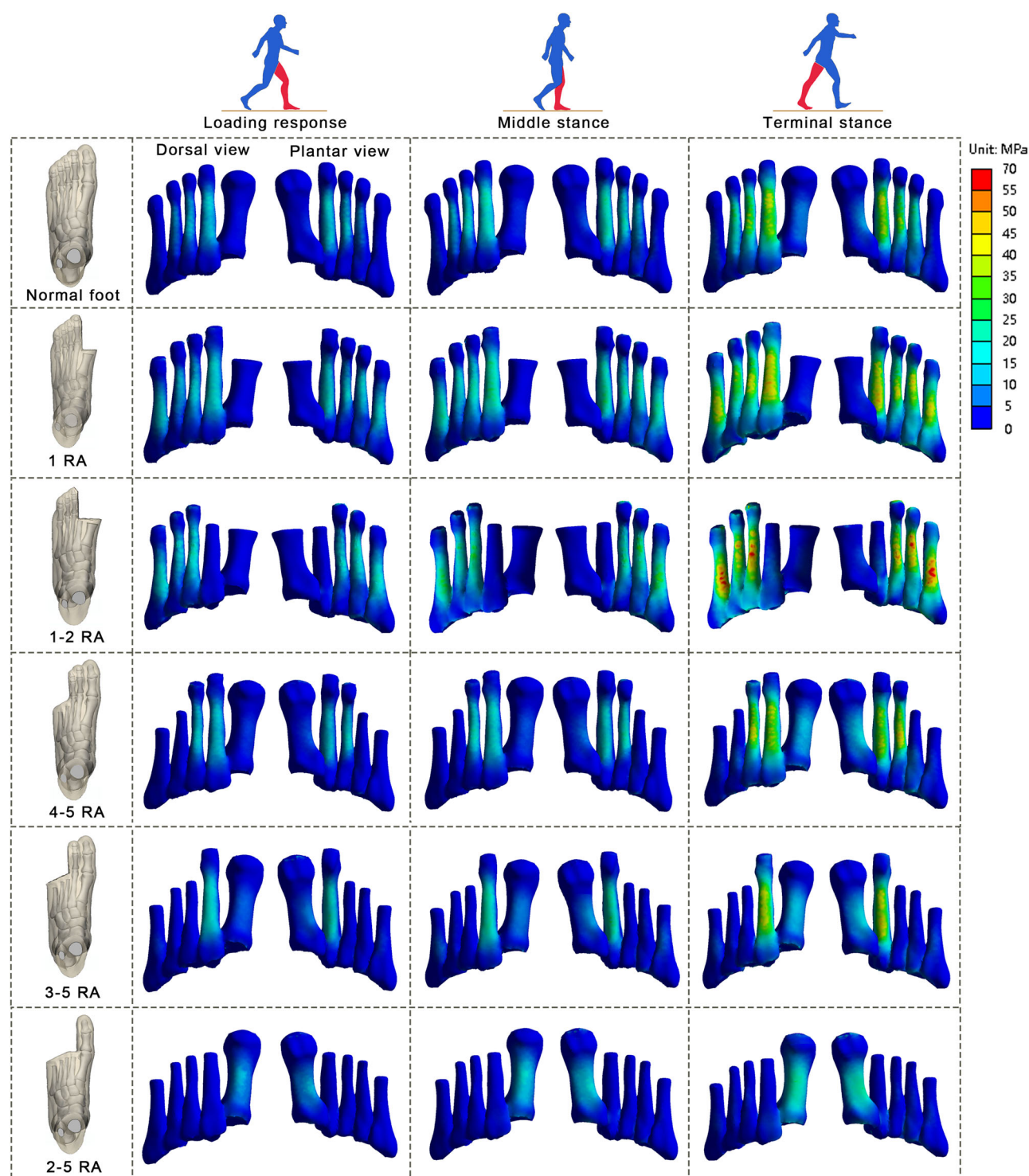


**Fig. 4 | The von Mises stress distribution of the five metatarsals in the phases of loading response, middle stance, and terminal stance.** The overall stress levels in the 1 ray amputation (RA) and 1-2 RA groups were markedly higher than those in other groups, with this disparity being particularly pronounced during the terminal stance phase.

IQR: 2.79–8.33 MPa) and 2nd (median: 21.97 MPa, IQR: 13.09–31.06 MPa) metatarsals (Fig. 5e).

In the 2-5 RA group, the majority of the load from the amputated rays was transferred to the 1st ray, resulting in a noticeable increase in the stress level of the 1st metatarsal. However, its absolute value still remained relatively low (median: 15.21 MPa, IQR: 10.86–19.42 MPa). Meanwhile, the stress levels of the 2nd to 5th metatarsals all decreased markedly (Fig. 5f).

From the comparison between each group and the normal foot group, it's evident that the metatarsals of amputated rays demonstrated a marked decline in stress levels, indicating that these amputated rays had a significant reduction in their load-bearing capabilities. In contrast, the remaining non-amputated metatarsals experienced elevated stress levels, indicative of the load being redistributed to these remaining rays. Overall, the 1 RA and 1-2 RA groups exhibited highest stress levels, suggesting that the soft tissues surrounding the non-amputated metatarsals in these groups are subjected

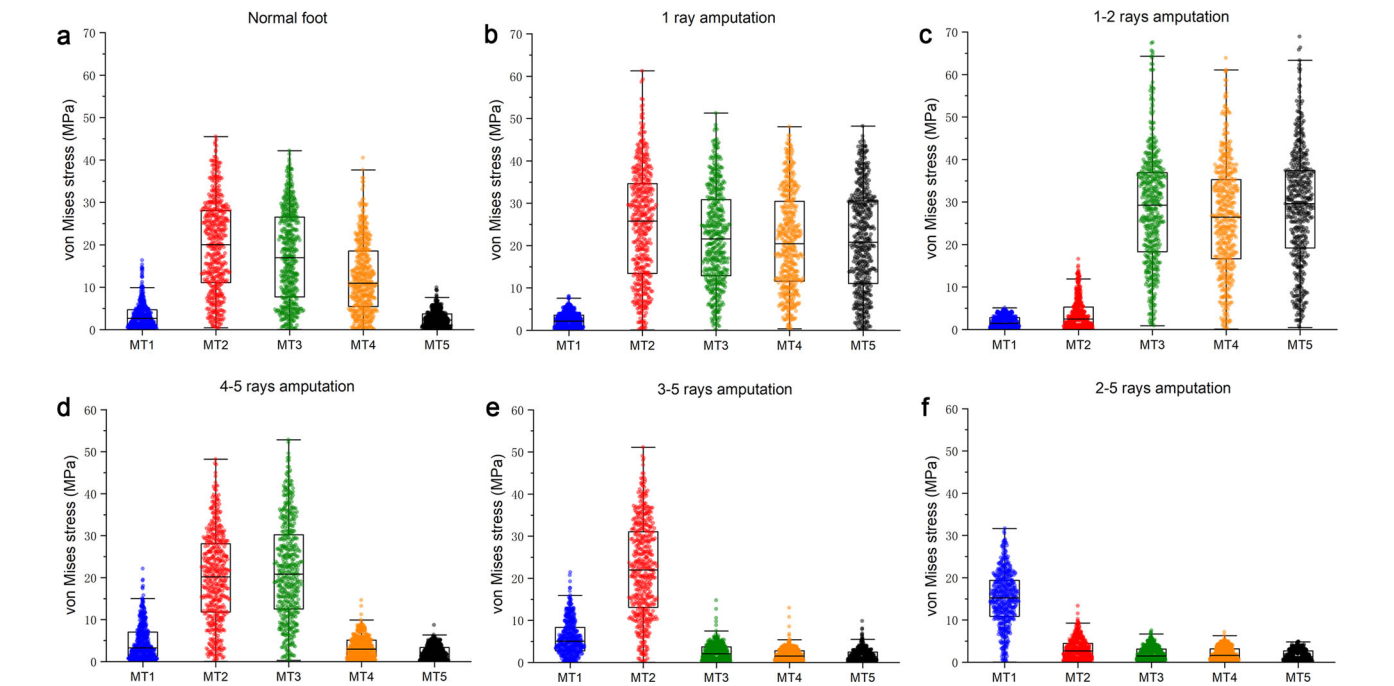


**Fig. 5 | The boxplots display the overall levels of von Mises stress on each metatarsal during the terminal stance phases. a** The von Mises stress distribution of the normal foot group. **b, c** Notably, the 1 ray amputation (RA) and 1-2 RA groups displayed the highest von Mises stress levels, indicating that the soft tissues surrounding the corresponding metatarsals in these groups are at a higher risk of reulceration. **d-f** In the 4-5 RA, 3-5 RA and 2-5 RA groups, the stress levels of the remaining non-amputated metatarsals did not show a marked increase. Each dot represents a value of von Mises stress recorded by the marked nodes. The box range of the boxplots extends from the 25% to the 75%, with the central line representing the median. The upper and lower dashed lines span from the 1.5% to the 98.5%.

**Table 2 | The von Mises stress of the five metatarsals**

	Normal	1 RA	1-2 RA	4-5 RA	3-5 RA	2-5 RA
MT 1	2.69 (1.16–4.69)	2.18 (0.82–3.59)	1.50 (0.64–2.81)	3.28 (1.32–7.06)	5.07 (2.79–8.33)	15.21 (10.86–19.42)
MT 2	20.03 (11.12–28.06)	25.79 (13.45–34.63)	2.50 (0.87–5.30)	20.18 (11.83–28.09)	21.97 (13.09–31.06)	2.69 (1.08–4.45)
MT 3	16.96 (7.73–26.54)	21.56 (12.88–30.86)	29.30 (18.31–36.91)	20.87 (12.54–30.23)	2.08 (0.83–3.73)	1.50 (0.70–3.13)
MT 4	10.95 (5.44–18.53)	20.47 (11.63–30.49)	26.46 (16.68–35.26)	2.98 (1.21–5.10)	1.53 (0.55–2.80)	1.65 (0.62–3.15)
MT 5	2.27 (1.05–3.70)	20.77 (11.08–30.56)	29.62 (19.21–37.40)	1.83 (0.66–3.36)	1.39 (0.45–2.50)	1.32 (0.60–2.65)

MT metatarsal, RA ray amputation.  
(MPa) (presented as median with interquartile range).

to a higher risk of reulceration. In the 1 RA group, the median stress for the 2nd through 5th metatarsals consistently exceeded 20 MPa. Meanwhile, in the 1-2 RA group, the 3rd to 5th metatarsals all had median stress values surpassing 25 MPa.

**Clinical case examples**

The results of the FE analysis showed that the 1 RA and 1-2 RA groups had significantly more danger areas on the plantar forefoot, which underscores the importance of preserving the first ray in preventing reulceration. Additionally, it indicated that amputating the second ray in addition to the first ray further increases the risk of reulceration. Two case examples from our institution were provided to support the FE analysis findings. All clinical images were obtained with the patients’ informed consent.

The first case presented in Fig. 6 showed a patient with RA performed on both feet after infected DFUs. After undergoing the 2-5

RA on the right foot, the patient remained ulcer-free at his 10-year follow-up although he still required custom-made shoes to protect his only remaining toe. The preservation of the first ray allowed for the maintenance of most of the weight-bearing function on the medial column of his right foot, enabling the patient to retain walking ability. However, the patient’s left foot, which had the 1-3 RA, developed two ulcers (each on the remaining 4th and 5th metatarsal heads) within a year post-surgery despite the usage of customized offloading orthotics, necessitating regular podiatric intervention to trim callosities, treat ulcers, and adjustment of offloading orthotics. Notably, the remaining 4th and 5th toes had also developed deformities (claw toes) from the transfer metatarsalgia and attritional injuries to the plantar metatarsophalangeal structures. In combination with the initial FE analysis results, it can be inferred that the load originally borne by the 1-3 rays was transferred to the 4-5 rays, causing an obvious increase of strain in



**Fig. 6 | A 62-year-old male patient with diabetic foot ulcers underwent the 2-5 rays amputation (RA) on the right foot with no reulceration observed during the 10 years post-surgery. The left foot underwent the 1-3 RA, with two sites of reulceration identified at the 1-year postoperative follow-up.**



**Fig. 7 | A case of reulceration following first ray amputation (1 RA). a** A 56-year-old female patient had first ray necrosis due to a severe diabetic foot ulcer (DFU). **b** The patient underwent the 1 RA. **c** Two months postoperatively, a reulceration occurred at the forefoot. **d** The recalcitrant ulcer lasted for 1 year despite the use of orthotics and treatments such as wound care and dressing changes. **e** The transferring load also led to dislocation of the second metatarsophalangeal joint (red arrow), the development of a claw toe in the third ray, and biomechanical disturbances of the foot. **f** The patient subsequently underwent further surgery to excise the ulcer and correct the forefoot biomechanics (excisional arthroplasty for the second metatarsophalangeal joint; Weil's osteotomy for the third and fourth metatarsals).



the plantar forefoot area corresponding to the 4-5 rays. Consequently, this area of soft tissue was more susceptible to reulceration.

The second case presented in Fig. 7 once again highlighted the importance of the load-bearing capacity of the first ray. This patient presented with an infected necrotic DFU of the big toe underwent the 1 RA. Despite the preservation of all the lesser toes, reulceration and biomechanical disturbances of the foot still occurred, necessitating further surgeries. This also corresponded to the results of the aforementioned FE analysis, which indicated that the load originally borne by the first ray was transferred to the 2-5 rays, resulting in an obvious increase of strain in the residual plantar forefoot area particularly at the 2nd metatarsal head which was consistent with findings in Figs. 2 and 3 as described earlier.

## Discussion

This study provides a comprehensive examination of the biomechanical repercussions following different types of RA procedure in patients with DFUs. The findings from this FE analysis combined with supportive illustrations from clinical case examples underscore the importance of

preserving the first ray in mitigating the risk of reulceration post-amputation. The FE analysis revealed that the 1 RA and 1-2 RA groups exhibited significantly more areas of high strain on the plantar forefoot, suggesting a correlation between the types of amputation and the redistribution of mechanical load across the foot. Specifically, the load transfer to the 2-5 rays following the amputation of the first ray led to a discernible increase in strain in the residual plantar forefoot areas, heightening the susceptibility to reulceration. Additionally, further removal of the second ray will increase the risk of reulceration even more. Similar to the results of the computational FE analysis, the clinical cases detailed in Figs. 6 and 7 also demonstrate the critical biomechanical role of the first ray or first two rays (medial column of the foot).

These findings align with some previous literature. García et al.<sup>17</sup> conducted a prospective clinical study involving 65 patients, reporting that the 1-2 RA was identified as a predictor of reulceration, while if the patient experienced only 1 RA, the pressure beneath the second metatarsal head was also observed to significantly increase. Likewise, an 11-year retrospective review by Borkosky et al.<sup>25</sup>, involving 59 patients, revealed that nearly 43% of

patients with DFU undergoing 1 RA progressed to a more proximal repeat amputation, despite initial healing. Consequently, the authors suggested that a more proximal level amputation, such as the TMA, should be considered at the initial presentation of DFU with necrosis of the first ray. The retrospective analysis by Suh et al.<sup>10</sup>, involving 59 patients, found that, compared to transmetatarsal amputation with free flap reconstruction (32 patients), preserving the first ray or the first two rays with free flap reconstruction (27 patients) provided significantly better ambulatory function.

To the best of our knowledge, this is the first FE analysis study to compare different types of RA, providing a more precise elucidation of the biomechanical impacts that various RAs have on the foot. Our findings not only support the clinical reports mentioned in the preceding paragraph but also challenge the notion<sup>15</sup> that 1 RA typically results in better outcomes whereas central RA was significantly associated with reulceration. In terms of clinical practice implications, our study underscores the importance of preserving the first ray or first two rays during the RA procedure. Conversely, in cases where the extent of infection or necrosis necessitates the removal of the first ray or first two rays, our findings indicate a significantly increased risk of reulceration for the remaining rays, suggesting that the TMA may be a more suitable option.

In this study, the von Mises stress values of the metatarsals remained below the safety margin of human bone (150 MPa)<sup>26</sup>. However, these values represent the mechanical response within a single gait cycle, and stress fractures result from the cumulative effect of multiple gait cycles (repetitive force)<sup>27,28</sup>. Thus, the levels of von Mises stress in the metatarsals warrant attention. In Fig. 5, the second and third metatarsals of a normal foot exhibit higher von Mises stress, aligning with the previous observation that the 2-3 metatarsals in a normal foot are most susceptible to stress fractures<sup>28,29</sup>. The first metatarsal, with its thicker and shorter structure, exhibited relatively low von Mises stress values (median: 15.21 MPa, IQR: 10.86–19.42 MPa) even in the 2-5 RA group. This characteristic makes it less susceptible to stress fractures, highlighting the first ray's pivotal role in distributing load<sup>18,19</sup>. Additionally, considering that the body weight (BW) of patients in this study aligns with the average for East Asian diabetic patients<sup>30</sup>, it stands to reason that in populations with higher body weight, the observed strain and stress values on the metatarsals might escalate.

While cadaver experiments are considered an effective method for validating FE models<sup>31</sup>, implementing such an approach in this study faced noticeable challenges. The anatomical features and material properties of soft tissues in processed cadaveric specimens can considerably differ from those in vivo, making it difficult to maintain uniformity across different specimens. Moreover, attaching strain gauges to the metatarsal bones without compromising the integrity of the surrounding soft tissues posed a challenge, where intact soft tissue encapsulation of the foot bones was required<sup>32</sup>. This study did not utilize CT images of amputated patients' feet for the FE analysis because the length of metatarsal bones preserved during RA procedures varies among individuals with DFUs<sup>13</sup>, and this would introduce interference and bias into the FE analysis. Instead, CT images from the normal feet of diabetic patients were used to maintain uniformity and minimize confounding bias.

The FE models in this study are based on static simulations, which do not fully capture the dynamic nature of human gait. Although dynamic simulation could provide a comprehensive analysis of the entire gait cycle, it demands a substantially larger computational processing power<sup>32</sup>. Hence, following the methods established in prior research<sup>32,33</sup>, our approach focused on strategically selected 5 key static phases of gait: HS, LR, MS, TS, TO. In addition, this study followed previously reported methods<sup>32,34</sup> to simplify muscle force simulation without considering potential variability in muscle force, due to the lack of standardized approaches. Trinler et al.<sup>35</sup> investigated the variability in muscle force throughout the gait cycle and found substantial differences in muscle force estimations between two standard musculoskeletal modeling environments (AnyBody and OpenSim). These findings underscore the current absence of a standardized method capable of accurately capturing such variability in foot FE models.

In this study, the 6 diabetic patients included in the FE analysis had similar body weights (Supplementary Table 1). Thus, we applied the same magnitude of muscle forces for all patients. Finally, the retrospective analysis of clinical case examples may not fully represent the wide spectrum of post-RA outcomes in the DFU population. Therefore, while the computational and clinical findings offer relevant insights, future studies with dynamic gait analysis and larger clinical sample sizes are warranted to better evaluate the impact of different RA procedures on foot biomechanics and ulcer recurrence. Additionally, foot pressure mapping data could be incorporated to further quantify these clinical parameters.

In the surgical management of DFUs, the preservation of the first ray or first two rays—given viable tissues allows for primary closure or secondary healing—should be a key consideration to prevent reulceration and maintain foot biomechanics. When the extent of infection or necrosis necessitates the resection of the first ray or first two rays, there is a significantly heightened risk of reulceration for the remaining rays, which suggests that TMA might be a more appropriate option.

## Materials and methods

### Model construction

This study was reviewed and approved by the Institutional Review Board of Yangpu Hospital (LL-2023-SCI-004) per the Declaration of Helsinki. Foot CT images of 6 diabetic patients were obtained from the image database of the Yangpu Hospital (GE Medical Systems 64-row spiral CT scanner, with the slice thickness of 0.5 mm). Details of patient demographics were described in Supplementary Table 1. The foot geometry was scanned in a non-weight-bearing condition and with the ankle joint positioned neutrally<sup>32</sup>. Images were segmented and processed in Mimics software (Materialise, Belgium). Thirty bones (tibia, fibula, talus, navicular, calcaneus, cuboid, 3 cuneiforms, 5 metatarsals, 2 sesamoids, 14 phalanges) and encapsulated soft tissue were included in the 3D foot model. The acquired models were then refined using 3-Matic software (Materialise, Belgium) (Fig. 1a–c).

In 3-Matic, the Cut function was employed to perform ray amputation process on each foot model, eventually generating six variations from each original model: Normal foot, 1 RA, 1-2 RA, 4-5 RA, 3-5 RA, and 2-5 RA ( $n = 6$ ). For each type of amputation, the amputation range was kept consistent, and the amputation level was referenced from prior literature<sup>36</sup>. The remeshing, wrapping, and smoothing processes eliminated unwanted sharp edges. Mesh quality was further guaranteed by regulating triangle edge length and height-to-base ratios, as well as removing sharp edges using the triangle filter<sup>37</sup>. To improve the accuracy of the model and allow for frictionless movement of the bones, cartilage layers were incorporated for 37 joints between 30 bones<sup>32</sup>. Ligaments, Achilles tendon, and plantar fascia were manually added as 1D linear truss elements to the model and located based on the anatomical landmarks and confirmation from a senior foot and ankle surgeon. The plantar fascia was represented by linking each head of the metatarsal bones to the medial calcaneal tubercle. Muscle forces from the soleus, lateral, and medial gastrocnemius muscles were applied to the Achilles tendon. A 3D solid plate was added to the model to represent the ground. The volume mesh was created via the tetrahedral element (Fig. 1d, e).

### Material properties, loads, and constraints

Material properties of foot bones, cartilage, ligaments, plantar fascia, and ground plate were regarded as isotropic and homogeneous. Elasticity was represented using two material constants: Young's modulus ( $E$ ) and Poisson's ratio ( $\nu$ ). Bone materials of tibia and fibula were assigned based the Hounsfield unit (HU) of CT images. The encapsulated soft tissue was set as nonlinear hyperelastic material, defined using the Mooney-Rivlin model (Fig. 1h)<sup>38</sup>. The element types and material properties employed were illustrated in Table 3.

In the scope of this investigation, one gait cycle was simulated as a sequence of 5 static phases: HS, LR (first peak), MS, TS (second peak), and TO (Fig. 1f, g)<sup>39–41</sup>. A vertical ground reaction force (GRF) was exerted on the



**Table 3 | Element types and material properties for model components**

Component	Element Type	Young's Modulus (E), MPa	Poisson's Ratio, $\nu$	Cross-section Area, mm <sup>2</sup>
Foot bones <sup>32,47</sup>	10-node tetrahedral	7300	0.3	/
Tibia and fibula <sup>31,48</sup>	10-node tetrahedral	$\rho = 0.916^* \text{ HU} + 114$ $E = 0.06^* \rho^{\wedge} 1.51$	0.3	/
Cartilage <sup>32,47</sup>	10-node tetrahedral	1	0.4	/
Ligament <sup>32,33</sup>	Truss	260	/	18.4
Plantar fascia <sup>33,47</sup>	Truss	350	/	58.6
Ground plate <sup>47</sup>	10-node tetrahedral	17000	0.4	/
Encapsulated soft tissue <sup>47,49</sup>	10-node tetrahedral	Hyperelastic (Mooney-Rivlin 5 parameter, $C_{10} = 0.08556 \text{ Nmm}^{-2}$ , $C_{01} = -0.05841 \text{ Nmm}^{-2}$ , $C_{20} = 0.03900 \text{ Nmm}^{-2}$ , $C_{11} = -0.02319 \text{ Nmm}^{-2}$ , $C_{02} = 0.00851 \text{ Nmm}^{-2}$ , $D_1 = 3.65273 \text{ mm}^2\text{N}^{-1}$ )		

inferior surface of the ground plate. Drawing on prior studies delineating magnitudes of the GRF<sup>40–42</sup>, the GRF values are correspondingly assigned to 5 gait phases as follows: 40% BW \* g (HS), 115% BW \* g (LR), 85% BW \* g (MS), 120% BW \* g (TS), 20% BW \* g (TO). The g denoted the gravitational acceleration, approximately 9.81 m/s<sup>2</sup>. The muscle forces of the gastrocnemius-and-soleus complex during the gait cycle were exerted through the pulling force of the Achilles tendon. As per previously reported data, the magnitude of the muscle forces was set as: 80 N (HS), 800 N (LR), 1200 N (MS), 2000 N (TS), 800 N (TO)<sup>34,35</sup>.

Throughout 5 phases, the upper borders of the fibula, tibia, and the soft tissue were fixed by constraining 6 degrees of freedom. The surface contact between bone and cartilage layers was assumed as frictionless. The inner surface of the encapsulated soft tissue was bonded to the neighboring bone surface. The friction coefficient between the ground plate and the foot plantar surface was set as 0.6<sup>22,43</sup>.

### Model solutions

The FE analysis was conducted in the ANSYS 2021 (ANSYS, USA). An analysis for mesh convergence was executed, with the criteria being a change in maximum von Mises stress of less than 5% under the TS condition, to ensure a sufficiently fine element discretization<sup>44</sup>. An analysis for mesh convergence was executed to guarantee a sufficiently fine element discretization. The outcome assessment metrics encompass the von Mises strain (equivalent strain) distribution across the plantar foot, and the von Mises stress (equivalent stress) distribution along the five metatarsals. For a more detailed analysis, the plantar foot was partitioned into forefoot, midfoot, and hindfoot segments (Fig. 1i); while the stress on each metatarsal was assessed individually. Further, a total of 80 nodes were marked on each metatarsal, serving for von Mises stress measurement at these precise locations (Fig. 1j).

For assessing the risk of reulceration following RA in the diabetic foot, it was determined that compressions persisting for around 10 min, in conjunction with soft tissue strain exceeding 0.5, significantly increased the risk of ulceration<sup>45,46</sup>. Accordingly, we designated the mean von Mises strain surpassing 0.5 as the “danger value” for reulceration. The plantar surface exhibiting danger values was defined as the “danger area” for reulceration. The percentage of the danger area to the total plantar foot area was termed the “danger area ratio”. Although repetitive loading over multiple gait cycles is clinically what leads to reulceration, this computational simulation of a single representative gait cycle still provides meaningful preliminary indicators of the risk of reulceration, thereby allowing for clinical extrapolation.

### Validation

This study did not employ cadaver experiments to validate the FE models, as the material properties of the soft tissues in processed cadaveric specimens can considerably differ from those in vivo, and maintaining uniformity in anatomical features and material properties across different specimens is challenging. Furthermore, attaching strain gauges to metatarsal bones without compromising

the integrity of the surrounding soft tissues would be difficult in this study context where intact soft tissue encapsulation of the foot bones is required.

The comparison of FE analysis results to clinical data is considered by some to be the ultimate validation<sup>31</sup>. This study has chosen case examples from our institutions to illustrate the results of the FE analysis.

### Statistical analysis

After applying Kolmogorov-Smirnov normality test, differences between groups were assessed by one-way analysis of variance (ANOVA). The levels of significance were as follows: \* $P < 0.05$ , \*\* $P < 0.01$ , and \*\*\* $P < 0.001$ ; NS, not significant. Analysis was performed with OriginPro 2021 (OriginLab, USA).

### Data availability

All data associated with this study are present in the paper or the supplementary information.

### Code availability

The code that supports the findings of this study is available from the corresponding author upon reasonable request.

Received: 17 October 2024; Accepted: 14 July 2025;

Published online: 06 August 2025

### References

- McDermott, K., Fang, M., Boulton, A. J. M., Selvin, E. & Hicks, C. W. Etiology, epidemiology, and disparities in the burden of diabetic foot ulcers. *Diab. Care* **46**, 209–221 (2022).
- Armstrong, D. G., Tan, T.-W., Boulton, A. J. M. & Bus, S. A. Diabetic foot ulcers: a review. *JAMA* **330**, 62–75 (2023).
- Satish Chandra, M., Kunal, C. C., Aditi, K. & Abha, M. Diabetic foot. *BMJ* **359**, j5064 (2017).
- Tan, J. H. et al. Costs of patients admitted for diabetic foot problems. *Ann. Acad. Med., Singap.* **44**, 567–570 (2015).
- International Diabetes Federation. The Diabetic Foot. Brussels, Belgium, International Diabetes Federation, 2020. Accessed 19 Aug 2024. Available from <https://www.idf.org/our-activities/care-prevention/diabetic-foot.html>.
- Armstrong, D. G., Boulton, A. J. M. & Bus, S. A. Diabetic Foot Ulcers and Their Recurrence. *N. Engl. J. Med.* **376**, 2367–2375 (2017).
- Dalla Paola, L. et al. Ulcer recurrence following first ray amputation in diabetic patients: a cohort prospective study. *Diab. Care* **26**, 1874–1878 (2003).
- Ron, I. et al. Risk factors for a failed transmetatarsal amputation in patients with diabetes. *J. Bone Jt. Surg. Am.* **105**, 651–658 (2023).
- Zhang, S. et al. Clinical outcomes of transmetatarsal amputation in patients with diabetic foot ulcers treated without revascularization. *Diab. Ther.* **10**, 1465–1472 (2019).

10. Suh, Y. C. et al. Is reconstruction preserving the first ray or first two rays better than full transmetatarsal amputation in diabetic foot? *Plast. Reconstr. Surg.* **143**, 294–305 (2019).
11. Arnold, P. B. & Orgill, D. P. Discussion: is reconstruction preserving the first ray or first two rays better than full transmetatarsal amputation in diabetic foot? *Plast. Reconstr. Surg.* **143**, 306–307 (2019).
12. Izumi, Y., Satterfield, K., Lee, S. & Harkless, L. B. Risk of reamputation in diabetic patients stratified by limb and level of amputation: a 10-year observation. *Diab. Care* **29**, 566–570 (2006).
13. Hong, C. C., Saha, S. & Pearce, C. J. Does a shorter residual first metatarsal length after first ray amputation in diabetic patients leads to poorer outcomes - A risk factor study. *Foot Ankle Surg. J. Eur. Soc. Foot Ankle Surg.* **29**, 228–232 (2023).
14. Sanz-Corbalán, I. Metatarsal head resections in diabetic foot patients: a systematic review. *J. Clin. Med.* **9**, 1845 (2020).
15. McGuire, J., Thomson, A. & Kennedy, P. G. The biomechanics of diabetic foot amputation. *Wounds* **33**, 231–236 (2021).
16. Molines-Barroso, R. J. et al. Analysis of transfer lesions in patients who underwent surgery for diabetic foot ulcers located on the plantar aspect of the metatarsal heads. *Diabet. Med.* **30**, 973–976 (2013).
17. García-Madrid, M. et al. Analysis of plantar pressure pattern after metatarsal head resection. Can plantar pressure predict diabetic foot ulceration? *J. Clin. Med.* **10**, 2260 (2021).
18. Lavery, L. A., Lavery, D. C. & Quebedeaux-Farnham, T. L. Increased foot pressures after great toe amputation in diabetes. *Diab. Care* **18**, 1460–1462 (1995).
19. Quebedeaux, T. L., Lavery, L. A. & Lavery, D. C. The development of foot deformities and ulcers after great toe amputation in diabetes. *Diab. Care* **19**, 165–167 (1996).
20. Wang, Y., Li, Z., Wong, D. W.-C., Cheng, C.-K. & Zhang, M. Finite element analysis of biomechanical effects of total ankle arthroplasty on the foot. *J. Orthop. Transl.* **12**, 55–65 (2018).
21. Malakoutikhah, H. & Latt, L. D. Disease-specific finite element analysis of the foot and ankle. *Foot Ankle Clin.* **28**, 155–172 (2023).
22. Shaulian, H., Gefen, A., Solomonow-Avnon, D. & Wolf, A. Finite element-based method for determining an optimal offloading design for treating and preventing heel ulcers. *Comput. Biol. Med.* **131**, 104261 (2021).
23. Jannel, A., Salisbury, S. W. & Panagiotopoulou, O. Softening the steps to gigantism in sauropod dinosaurs through the evolution of a pedal pad. *Sci. Adv.* **8**, eabm8280 (2022).
24. Mann, R. A., Poppen, N. K. & O’Konski, M. Amputation of the great toe. A clinical and biomechanical study. *Clin. Orthop. Relat. Res.* 192–205 (1988).
25. Borkosky, S. L. & Roukis, T. S. Incidence of repeat amputation after partial first ray amputation associated with Diabetes Mellitus and Peripheral Neuropathy: An 11-Year Review. *J. Foot Ankle Surg.* **52**, 335–338 (2013).
26. Currey, J. D. Mechanical properties of vertebrate hard tissues. *Proc. Inst. Mech. Eng. H.* **212**, 399–411 (1998).
27. Warden, S. J., Davis, I. S. & Fredericson, M. Management and prevention of bone stress injuries in long-distance runners. *J. Orthop. Sports Phys. Ther.* **44**, 749–765 (2014).
28. Pathria, M. N., Chung, C. B. & Resnick, D. L. Acute and stress-related injuries of bone and cartilage: pertinent anatomy, basic biomechanics, and imaging perspective. *Radiology* **280**, 21–38 (2016).
29. Welck, M. J., Hayes, T., Pastides, P., Khan, W. & Rudge, B. Stress fractures of the foot and ankle. *Injury* **48**, 1722–1726 (2017).
30. Nam, G. E. et al. Body weight variability and the risk of cardiovascular outcomes and mortality in patients with Type 2 Diabetes: A Nationwide Cohort Study. *Diab. Care* **43**, 2234–2241 (2020).
31. Lewis, G. S., Mischler, D., Wee, H., Reid, J. S. & Varga, P. Finite element analysis of fracture fixation. *Curr. Osteoporos. Rep.* **19**, 403–416 (2021).
32. Moayedi, M., Arshi, A. R., Salehi, M., Akrami, M. & Naemi, R. Associations between changes in loading pattern, deformity, and internal stresses at the foot with hammer toe during walking; a finite element approach. *Computers Biol. Med.* **135**, 104598 (2021).
33. Wang, M., Li, S., Teo, E. C., Fekete, G. & Gu, Y. The influence of heel height on strain variation of plantar fascia during high heel shoes walking-combined musculoskeletal modeling and finite element analysis. *Front. Bioeng. Biotechnol.* **9**, 791238 (2021).
34. Kharazi, M., Bohm, S., Theodorakis, C., Mersmann, F. & Arampatzis, A. Quantifying mechanical loading and elastic strain energy of the human Achilles tendon during walking and running. *Sci. Rep.* **11**, 5830 (2021).
35. Trinler, U., Schwameder, H., Baker, R. & Alexander, N. Muscle force estimation in clinical gait analysis using AnyBody and OpenSim. *J. Biomech.* **86**, 55–63 (2019).
36. Fábio Carlos Lucas de, O. et al. Association between the level of partial foot amputation and gait: a scoping review with implications for the minimum impairment criteria for wheelchair tennis. *Br. J. Sports Med.* **57**, 237 (2023).
37. Mao, W. et al. Positive medial cortical support versus anatomical reduction for trochanteric hip fractures: Finite element analysis and biomechanical testing. *Comput Methods Prog. Biomed.* **234**, 107502 (2023).
38. Oddes, Z. & Solav, D. Identifiability of soft tissue constitutive parameters from in-vivo macro-indentation. *J. Mech. Behav. Biomed. Mater.* **140**, 105708 (2023).
39. Lieberman, D. E. et al. Foot strike patterns and collision forces in habitually barefoot versus shod runners. *Nature* **463**, 531–535 (2010).
40. Veltink, P. H., Liedtke, C., Droog, E. & van der Kooij, H. Ambulatory measurement of ground reaction forces. *IEEE Trans. neural Syst. rehabilitation Eng. : a Publ. IEEE Eng. Med. Biol. Soc.* **13**, 423–427 (2005).
41. Kowalski, E., Catelli, D. S. & Lamontagne, M. A waveform test for variance inequality, with a comparison of ground reaction force during walking in younger vs. older adults. *J. Biomech.* **127**, 110657 (2021).
42. Shaw, J. E., van Schie, C. H., Carrington, A. L., Abbott, C. A. & Boulton, A. J. An analysis of dynamic forces transmitted through the foot in diabetic neuropathy. *Diab. Care* **21**, 1955–1959 (1998).
43. Zhang, M. & Mak, A. F. T. In vivo friction properties of human skin. *Prosthet. Orthot. Int.* **23**, 135–141 (1999).
44. Yang, A.-L. et al. Computational evaluation of the axis-blade angle for measurements of implant positions in trochanteric hip fractures: A finite element analysis. *Comput. Biol. Med.* **158**, 106830 (2023).
45. Loerakker, S. et al. The effects of deformation, ischemia, and reperfusion on the development of muscle damage during prolonged loading. *J. Appl. Physiol.* **111**, 1168–1177 (2011).
46. Luboz, V. et al. Influence of the Calcaneus Shape on the Risk of Posterior Heel Ulcer Using 3D Patient-Specific Biomechanical Modeling. *Ann. Biomed. Eng.* **43**, 325–335 (2015).
47. Zhang, Y. et al. Effects of severe hallux valgus on metatarsal stress and the metatarsophalangeal loading during balanced standing: A finite element analysis. *Comput. Biol. Med.* **97**, 1–7 (2018).
48. Manual, FEA/CFD: Material Expressions. *Mimics Medical 21.0 Reference Guide*.
49. Qiu, T.-X., Teo, E.-C., Yan, Y.-B. & Lei, W. Finite element modeling of a 3D coupled foot–boot model. *Med. Eng. Phys.* **33**, 1228–1233 (2011).

## Acknowledgements

We thank Shou-Chao Du and Sun-Jun Hu from Tongji University for providing relevant clinical insights. No funding was granted for the study. Please contact Wei Mao (first corresponding author) for the most timely and accurate responses regarding the study.

## Author contributions

Conceptualization: W.M., D.J.J., Y.Q.Z., C.C.H.; Methodology: M, D.J.J., Y.Q.Z., W.T.J.; Investigation: W.M., D.J.J., Y.Q.Z., K.Y.S.L., Y.M.Q.; Visualization: W.M., D.J.J., K.Y.S.L., Y.M.Q.; Project administration: Y.Q.Z., W.T.J., C.C.H.; Supervision: W.T.J., S.M.C., C.C.H.; Writing – original draft: W.M., D.J.J., Y.Q.Z., S.M.C.; Writing – review & editing: Y.Q.Z., W.T.J., C.C.H.

## Competing interests

The authors declare no competing interests.

## Additional information

**Supplementary information** The online version contains supplementary material available at

<https://doi.org/10.1038/s41746-025-01891-w>.

**Correspondence** and requests for materials should be addressed to Wei Mao, Wei-Tao Jia or Choon Chiet Hong.

**Reprints and permissions information** is available at <http://www.nature.com/reprints>

**Publisher's note** Springer Nature remains neutral with regard to jurisdictional claims in published maps and institutional affiliations.

**Open Access** This article is licensed under a Creative Commons Attribution-NonCommercial-NoDerivatives 4.0 International License, which permits any non-commercial use, sharing, distribution and reproduction in any medium or format, as long as you give appropriate credit to the original author(s) and the source, provide a link to the Creative Commons licence, and indicate if you modified the licensed material. You do not have permission under this licence to share adapted material derived from this article or parts of it. The images or other third party material in this article are included in the article's Creative Commons licence, unless indicated otherwise in a credit line to the material. If material is not included in the article's Creative Commons licence and your intended use is not permitted by statutory regulation or exceeds the permitted use, you will need to obtain permission directly from the copyright holder. To view a copy of this licence, visit <http://creativecommons.org/licenses/by-nc-nd/4.0/>.

© The Author(s) 2025, corrected publication 2025